EDGE-PLASMA PROPERTIES OF THE UCLA TOKAMAKS

S.J. ZWEBEN*, R.J. TAYLOR
Center for Plasma Physics and Fusion Engineering,
University of California,
Los Angeles, California,
United States of America

ABSTRACT. Probe measurements of the edge plasmas of the Macrotor and Microtor tokamaks are described. Limiter scrape-off layer thicknesses as measured with Langmuir probes are for Macrotor $\lambda \cong 7-10$ cm and for Microtor $\lambda \sim 1$ cm, both values being consistent with the Bohm diffusion rate. Heat deposition measured with thermocouples attached to small probes shows an anomalously high heat flux, particularly from the electron drift direction. It is argued that the anomalous particle diffusion is most likely associated with the large edge density fluctuations, while the anomalous heat flux is most likely due to a directed high-energy electron population.

1. INTRODUCTION

Heat and particle flows at the edge of present-day tokamak plasmas are not routinely diagnosed and not very well understood. These flows determine the plasma–wall and/or plasma–limiter interaction and play an important role as a boundary condition for plasma confinement and impurity control. The prediction and control of edge heat and particle flows in future reactor-grade tokamaks will be important for optimizing divertor efficiency [1] or for possible divertorless operation [2].

Present-day tokamak edge plasmas are relatively cold and low in density ($n_e \approx 10^{11}-10^{13}\,cm^{-3}$, $T_e \sim 5-50$ eV) and so are most easily diagnosed with probes. This paper describes probe measurements in the edge regions of the two UCLA tokamaks: Macrotor ($R = 90$ cm, $a = 45$ cm, $B_T = 0.2-0.3$ T, $T_{e0} \sim 100$ eV, $\bar{n}_e < 2 \times 10^{13}\,cm^{-3}$) and Microtor ($R = 30$ cm, $a = 10$ cm, $B_T = 2$T, $T_{e0} \sim 500$ eV, $\bar{n}_e < 2 \times 10^{14}\,cm^{-3}$). Both tokamaks are routinely titanium coated and have very low impurity levels ($Z \cong 1$). Both machines are constructed with thick walls and are normally operated without localized limiters; however, for these experiments, various limiters have been inserted to examine specific plasma–limiter interactions.

These types of measurements can provide a useful empirical knowledge of the edge-plasma density, temperature, fluctuation levels and heat flux. We neglect here the atomic physics processes (ionization, recombination, sputtering, etc.) which will eventually have to be measured and correlated with the plasma properties for a clear understanding of the tokamak edge.

2. EXPERIMENTAL DETAILS

The probe used for most of these experiments had a single cylindrical stainless steel tip with radius 0.15 cm, exposed length 0.5 cm, total exposed area $\cong 0.5\,cm^2$, and tip mass $\cong 0.6$ g. The tip was biased typically −70 V DC in order to measure the ion saturation current I^+ (monitored by the voltage drop across a $10-100\,\Omega$ series resistor); the same tip also had mounted within it an iron/constantin thermocouple which was used to measure the rise in tip temperature caused by the plasma discharge. This probe was radially movable and was mounted at the end of a 0.6 cm diameter grounded steel shaft. The ceramic insulation between tip and shaft was recessed so that it did not touch the plasma (since ceramics tended to crack under the highest plasma heat flux levels).

The current drawn by the probe tip when it is biased in the ion saturation region of its characteristic, I^+, can be related to the local plasma density by [3–5]

$$I^+ = \frac{ne\bar{v}_i A}{4} \qquad (1)$$

where A is the effective area for ion collection and

$$\bar{v}_i \cong \sqrt{\frac{8}{\pi}\,\frac{kT_e}{M_i}}$$

* Present address: Department of Applied Physics, 128–95, Caltech, Pasadena, CA.91125, USA.

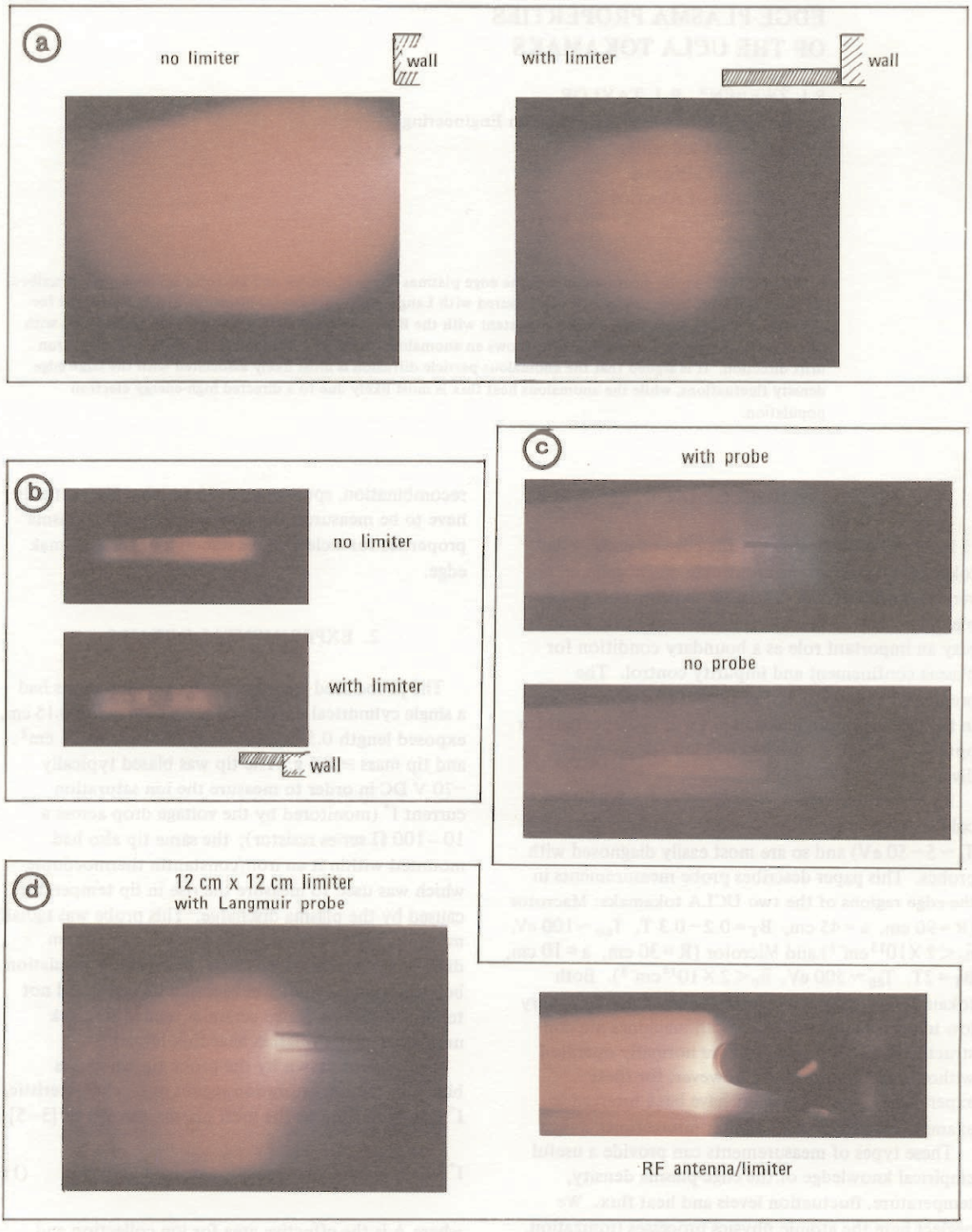

FIG. 1. Open-shutter photographs of the edge plasma taken from a bottom port (outer wall at right): (a) with and without a limiter in Macrotor; (b) in Microtor; (c) with and without a large probe in Macrotor; (d) at limiters in Macrotor. The limiters in (a) and (b) are both ~180° toroidally away from this view port and extend 30 cm and 3 cm, respectively, inward past the wall.

is average ion speed. For a typical cylindrical probe radius $r_p \cong 0.15$ cm we have for either tokamak at $n \sim 10^{12}\,cm^{-3}$, $r_p/\lambda_D \sim 50$ (where λ_D is the Debye length), so that the small sheath [3] approximation is valid. Thus the effective area for ion collection is taken to be the 'projected' probe area or $2/\pi$ times the total probe area for the strong magnetic field case of Microtor [6], since $r_p/\rho_i \sim 10$ (where ρ_i is the ion gyroradius); however, for Macrotor we use the full probe area since $r_p/\rho_i \sim 1$. Considering the uncertainties in estimating A and T, we cannot obtain the absolute density from Eq.(1) to better than a factor of about three uncertainty; however, the measurement of relative density versus position should be much more reliable. For many purposes the ion current I^+ or the current density $J^+ = I^+/A$ is itself more relevant for the edge plasma than either n or T separately, e.g. for sputtering, heat flux or particle pumping applications for which the incident ion flux is important.

Heat deposition onto this probe has been measured using the thermocouple inside the probe tip: typical temperature rises of $10-100°C$ are measured after each shot on a strip-chart recorder. Since the thermally insulated probe tip cools quite slowly after the discharge, it is straightforward to calculate the total heat Q deposited onto the probe tip by using the measured temperature rise, tip mass and the specific heat of steel. The total heat Q deposited onto the probe tip throughout the whole discharge can be estimated to within better than a factor-of-two accuracy in this way (limited by some uncertainty in the effective thermal mass of the tip). The average heat flux $\bar{q}$ in $W \cdot cm^{-2}$ is obtained by dividing the total heat Q by the effective probe area and the discharge duration.

Probes like this can usually be inserted well past the limiter in these tokamaks without damaging the probes or affecting the global properties of the discharge [7–9], and previous two-probe correlation studies in Macrotor have also indicated that the local plasma properties are not significantly perturbed by such small probes. However, the details of the local probe environment are still to some extent uncertain; for example, recycling (hence local plasma cooling) or impurity influx can occur at the probe, and abnormal conditions such as arcing, disruptions and runaway impact can melt or evaporate parts of the probe tip. It is also true that if the probes are inserted too far, the discharge impurity level increases and the plasma is perturbed. However, for the measurements described here (which were usually confined to the limiter shadow region), the probe did not affect the discharge or the impurity level and it did give results which are consistent with other diagnostic information (e.g. interferometer and UV emission measurements [10]). Thus we are led to assume that this probe was sampling the plasma in an approximately non-perturbative way; in particular, the current drawn by these small probes does not change the local ion saturation current as monitored by another probe nearby, and the heat and particle fluxes to the probe were a negligible ($<1\%$) fraction of the overall tokamak heat and particle flows.

Two other types of probes were also used in these experiments. One was actually a set of four fixed probes which were mounted in the side of a Microtor limiter (see Section 4.1), and the other was a large-area double-sided probe which was used to measure heat flux asymmetries in both Macrotor and Microtor (see Section 4.3). The principles of operation for these probes are the same as those just described for the single Langmuir/thermocouple probe.

Open-shutter photographs of some probes and limiters in the edge plasma are shown in Fig.1; (a) and (b) show the effect of limiters on the visible emission in their scrape-off layers; as shown in (c), the presence of the large 2 cm × 5 cm double-sided probe in limiterless discharge is accompanied by only a slight increase in recycling light at its surface; (d) shows the large light emission due to recycling at the limiters.

3. SCRAPE-OFF LAYER THICKNESSES

An empirical knowledge of the scrape-off layer thickness may be useful for the design of limiters, RF antennas or for impurity studies [11, 12]. We describe probe measurements in the limiter scrape-off regions of Macrotor and Microtor in Sections 3.1 and 3.2; Section 3.3 describes measurements in a limiterless Macrotor discharge, and in Section 3.4 particle diffusion coefficients are estimated from the scrape-off layer measurements. The possible causes of this diffusion are discussed in Section 6.2.

3.1. Macrotor

Typical ion saturation current signals I^+ for a low-density and a high-density Macrotor discharge are shown in Fig.2. In both cases the 0.15 cm radius probe (as described in Section 2) was $\lesssim 2$ cm toroidally away from and 1 cm radially behind the edge of the 12 cm high grounded copper outer limiter (see Fig.2(c)), which for this particular run was 19 cm from the outer

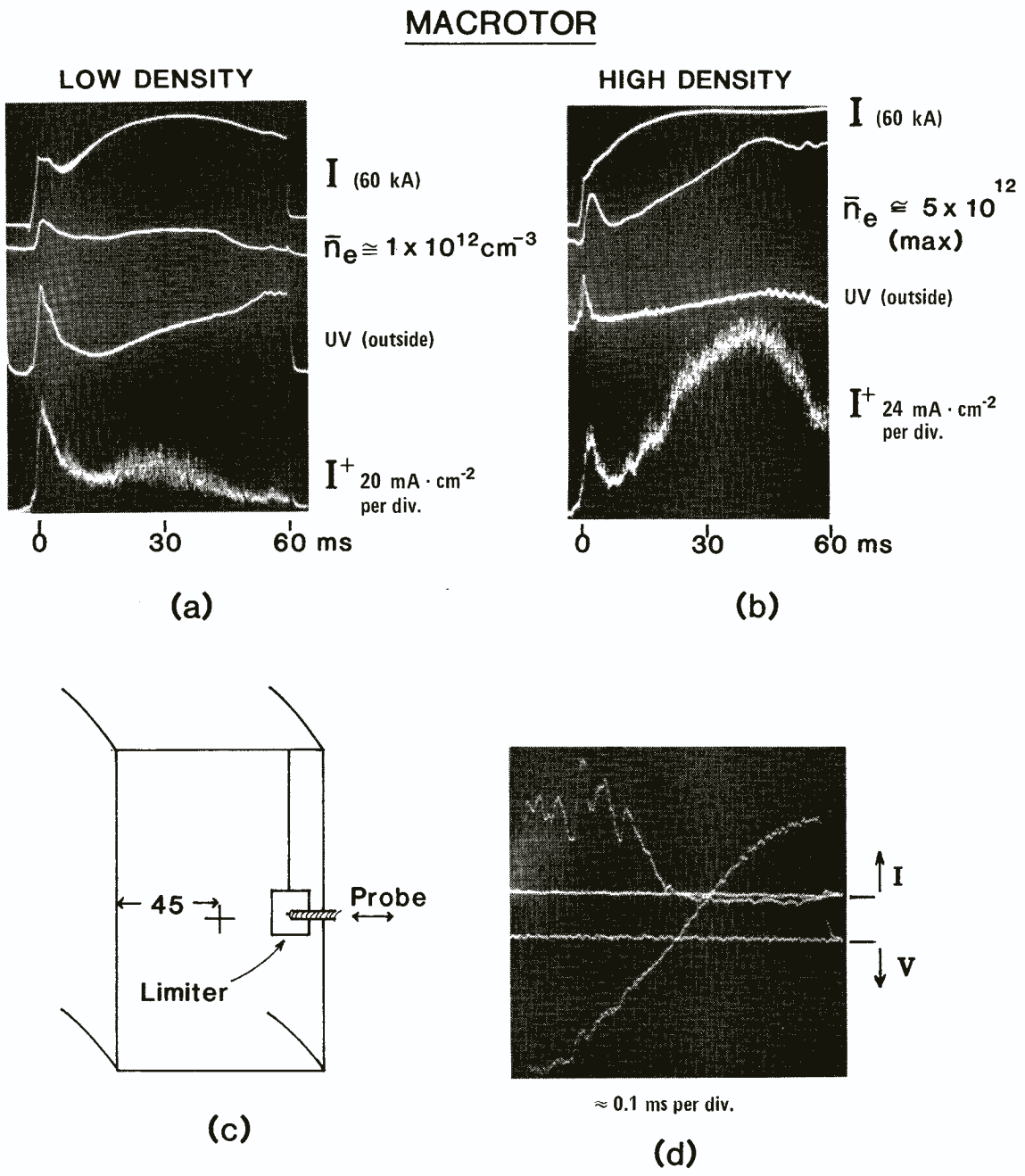

FIG.2. Ion saturation currents I^+ versus time for low-density (a) and high-density (b) Macrotor discharges. The probe for these cases is positioned ≅ 1 cm radially behind the 12 cm × 12 cm grounded limiter, as shown in (c). An (I,V) sweep from +120 to −120 V (sinusoidally) is shown in (d). The probes for ion saturation current measurements were biased by −70 V.

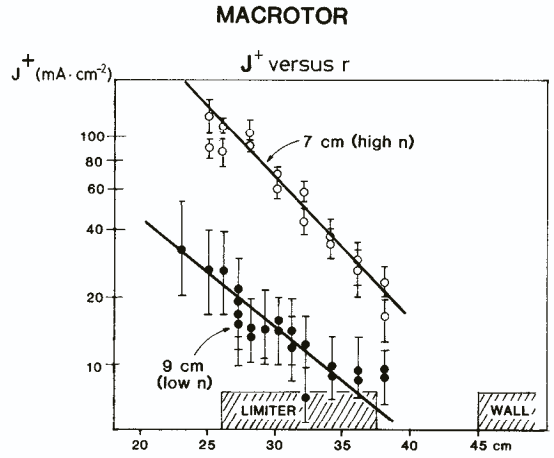

FIG.3. Ion saturation current density J^+ versus radius as measured at $t \cong 30$ ms by a probe near the limiter (as shown in Fig.2(c). The e-folding lengths of J^+ in the scrape-off layer of Macrotor are $\lambda = 7-9$ cm.

wall at the equatorial plane. As can be seen in (a) and (b), the signals I^+ generally follow the evolution of $\bar{n}_e$ as measured through the centre of the discharge by the interferometer; however, as in the case of the low-density discharge at $t \gtrsim 30$ ms, a decrease in I^+ at the probe can also be caused by a small inward movement of the plasma.

Figure 2(d) shows a typical Langmuir probe (I, V) sweep, taken in this case at $t \cong 30$ ms during a discharge like that of Fig.2(a). The temperature and space potential of the plasma can be inferred from this sweep (see Section 4); however, at this point we just note that the −70 VDC bias used for the probe in Fig.2(a, b) puts the probe well within the ion saturation part of the (I, V) characteristic.

A general feature which is evident from the I^+ photographs of Fig.2 is the large and ever present fluctuation level. For Macrotor, these broadband fluctuations are mainly at $f < 100$ kHz and have $\tilde{I}^+/I^+ \sim 0.05-0.3$ [7–8]. In these photos the general trend of $\tilde{I}^+/I^+$ decreasing with increased density can also be seen. Some details of these fluctuations are given in Section 5; for the remainder of this section we deal only with the mean values of I^+ as averaged over typically ~1 ms.

In Fig.3 we plot $J^+ = I^+/A$ ($A = 0.5$ cm^2) versus the radial position of this same probe for the two types of discharges shown in Fig.2(a, b). The most interesting information contained in this plot is the scrape-off layer thickness 'λ', defined here as the e-folding length of the decay of J^+ in the shadow of the limiter (the density and temperature scrape-off thicknesses are referred to as λ_n and λ_T respectively). For the high-density case we find $\lambda \cong 7$ cm and for the low-density case we find $\lambda \cong 9$ cm. This rough invariance of λ with n (with a slight trend toward larger λ at lower n) is a general feature of these measurements on both machines.

The absolute density can be estimated from J^+ using Eq.(1). Although the probe is only 1–2 cm away toroidally from the limiter, we take 'A' to be the whole exposed probe area, since $\rho_i \sim 0.2$ cm $\sim r_p$ (note that J^+ versus r increases smoothly through the limiter edge at $r = 26$ cm). Unfortunately, in Macrotor the edge fluctuations are so large that an accurate estimate of T_e from the Langmuir probe (I, V) sweep is difficult (see Fig.2(d)); however, for an estimated $T_e = 20$ eV near the limiter edge at $t \cong 30$ ms, we find $n \cong 4 \times 10^{11}$ cm^{-3} at this location for the high-density case. This is reasonable when compared with the line-averaged density $\bar{n}_e = 4 \times 10^{12}$ cm^{-3} also measured at this time.

Another set of measurements was made in order to check whether λ was dependent on the toroidal distance from the limiter. The same 0.15 cm radius probe was scanned at the outer equatorial plane, 120° toroidally away from a grounded limiter similar to that of Fig.2(c), and a scrape-off layer thickness $\lambda \cong 10$ cm was observed. This approximate independence of λ on toroidal angle was also observed in Microtor.

3.2. Microtor

The Microtor tokamak has a much smaller minor radius and a much larger toroidal field than the Macrotor tokamak. Measurements of J^+ were made using the same 0.15 cm radius probe in the scrape-off layer of Microtor ($A \cong 0.3$ cm^2 was assumed since $\rho_i \ll r_p$). The results showed typically $\lambda \cong 1$ cm for a grounded rail limiter positioned horizontally at the outside of the chamber approximately independent of $\bar{n}$ over the range 5×10^{12} cm$^{-3} \leqslant 5 \times 10^{13}$ cm^{-3}. The general character of the I^+ signal observed in the scrape-off layer of Microtor, i.e. its dependence on plasma density and positioning and its large turbulent fluctuation level, was very similar to that observed in Macrotor (Fig.2).

Figure 4 shows a comparison of the scrape-off layer J^+ radial profiles for two limiter configurations, one in which a rail limiter was extended poloidally at the outside and another for which the same limiter was rotated by 90° so as to extend toroidally at the outside (the rail was shaped to fit the curvature of

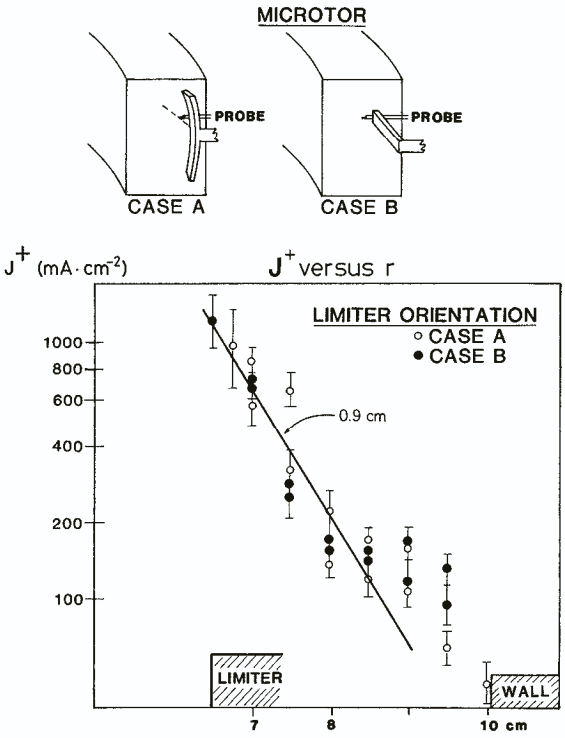

FIG.4. Ion saturation current density J^+ versus radius as measured in the limiter scrape-off layer in Microtor. The limiter is inserted radially 3 cm from the wall and grounded for both cases. The scrape-off thickness is $\lambda \cong 1$ cm for both orientations of this rail limiter.

the outer wall). It was found that nearly identical plasmas could be run with these two configurations and that for both cases $\lambda \cong 1$ cm (see Section 3.4 for discussion of this result).

An estimate of local edge density can be made through Eq.(1) using the measured $J^+ \cong 1$ A·cm^{-2} and $T_e \cong 25$ eV near the limiter edge (see Fig.6), which shows that in this edge region $n \cong 3 \times 10^{12}$ cm^{-3} for Microtor. This can be compared with $\bar{n}_e \cong 5 \times 10^{13}$ cm^{-3} line-averaged density measured at this time.

3.3. Limiterless case

Figure 5(a) is a plot of J^+ versus radius as measured at $t \cong 30$ ms in a limiterless Macrotor discharge using the same 0.15 cm radius probe as for the limiter cases of Section 3.1. Somewhat surprisingly, the e-folding length of the edge plasma J^+ profile is not much different from that observed in the scrape-off layer for the limiter cases, i.e. $\lambda \cong 10$ cm. This profile is somewhat sensitive to plasma positioning; for example, a very flat J^+ profile was observed when the plasma was shifted radially inward. Note that the absolute values of J^+ are $\simeq 5$ times larger in the limiterless cases, which is in part due to the $\cong 3$ times higher $\bar{n}_e$ allowed by the removal of the limiter.

Also, Fig.5(b) shows photographs of I^+ with fluctuations similar to those seen behind the limiter in Fig.2. A particularly smooth (I,V) probe sweep made at r = 31 cm (where $\tilde{I}^+/I^+$ is relatively small) indicates $T_e \cong 30 \pm 5$ eV in this case (Fig.5(c)).

3.4. Estimate of particle diffusion coefficient

We have found for rail limiters that the scrape-off thickness of J^+ was $\lambda \sim 7-10$ cm for Macrotor and $\lambda \sim 1$ cm for Microtor. It is interesting to translate this information into a radial particle diffusion coefficient $D_\perp$ for ions in the shadow of the limiter by using a 1-D scrape-off model in which (see, for instance, Refs [13–15])

$$D_\perp = \lambda^2/\tau_\parallel \qquad (2)$$

where $\tau_\parallel$ is defined as the average residence time of an ion in the scrape-off layer. Using $\tau_\parallel = 4L/\bar{v}_i$ ($\bar{v}_i$ is defined below Eq.(1)) and $L = q\pi R$ (see below) for the average length along the field line which the ion in the scrape-off layer travels before it intersects the limiter, we find:

$$D_\perp \sim 10^5 \text{ cm}^2 \cdot \text{s}^{-1} \text{ (Macrotor)}$$
$$D_\perp \sim 5 \times 10^3 \text{ cm}^2 \cdot \text{s}^{-1} \text{ (Microtor)} \qquad (3)$$

These values are $\sim 2D_{Bohm}$ for Macrotor and $\sim 0.5 D_{Bohm}$ for Microtor.

The construction of diffusion coefficients such as in Eq.(3) is subject to several uncertainties: (1) The length L is not measured and could actually be anywhere from $\sim q\pi R/2$ (if the field lines at the limiter intersect the inner wall of the machine) to $\sim 20\pi R$ (for the partial rail limiter of Fig.2(c)); (2) ion viscosity or charge-exchange effects could limit the effective L to less than the geometrical field line length ($\lambda_{ii} \cong 100$ cm at $n_i = 10^{12}$ cm^{-3} and $\lambda_{i0} \cong 1000$ cm at $n_0 \sim 10^{11}$ cm^{-3}); (3) possible ionization and recombination within the scrape-off layer and recycling or reflection at the limiter are neglected; (4) the plasma flow velocity should be used in $\tau_\parallel$ instead of an ion thermal velocity $\bar{v}_i/4$.

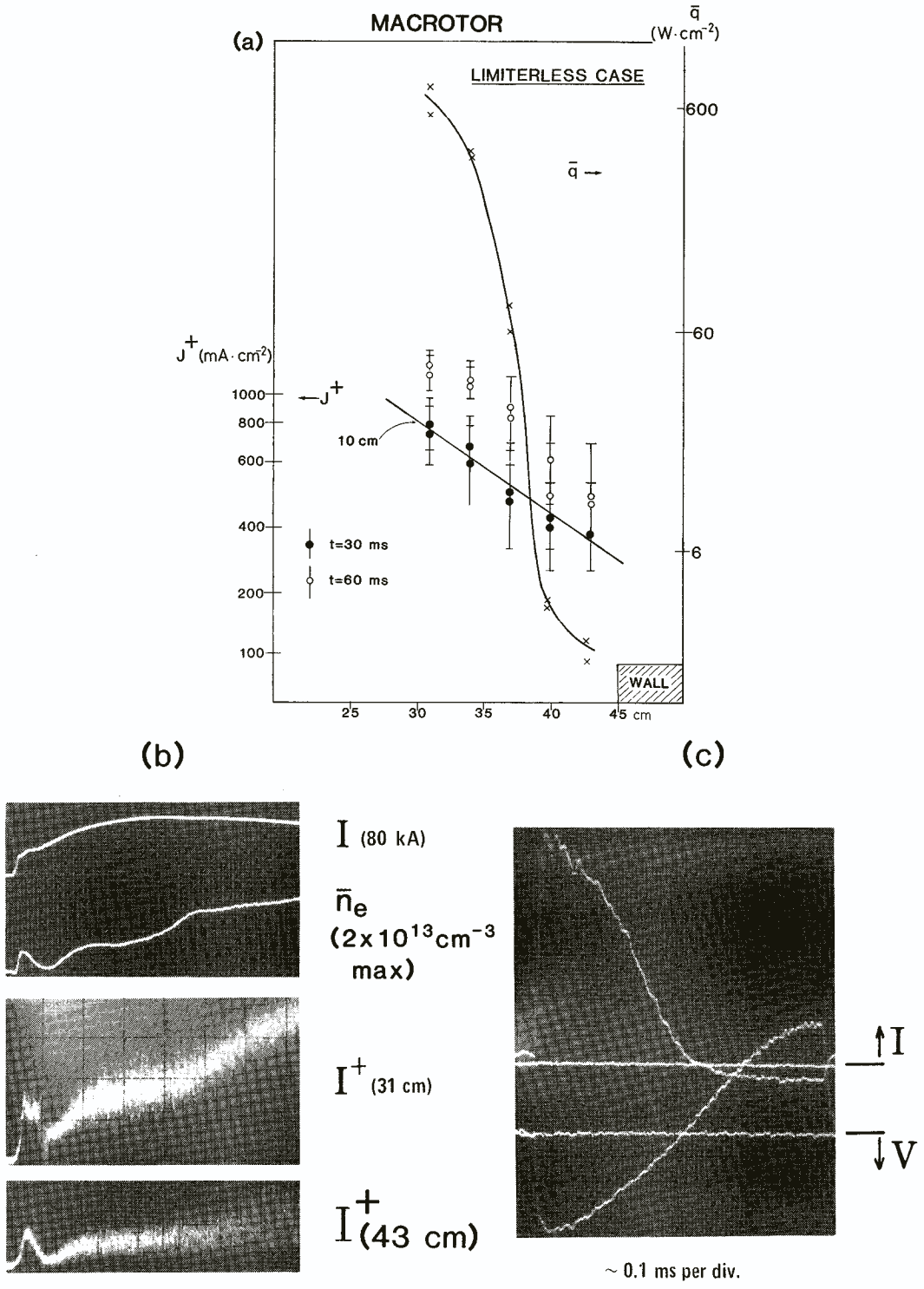

FIG.5. (a) J^+ versus r for a limiterless Macrotor discharge; (b) and (c): photos of I^+ and an (I, V) sweep, which show features similar to those measured in the limiter shadow in Fig.3. (The heat measurements of $\bar{q}$ are discussed in Section 4.2.)

Thus these diffusion coefficients are only order-of-magnitude estimates. It may be merely coincidental that $D_\perp \sim D_{Bohm}$; however, the data do show a trend which seems consistent with that expected for Bohm-type diffusion, namely that $D_\perp$ is approximately independent of n over a factor of four in both machines.

A dependence of λ on the limiter configuration would be expected from Eq.(2), namely as L increases, λ should also increase. For the comparison of two limiters shown in Fig.4, the partial toroidal limiter of toroidal length T and height H inclined at an angle $\theta \cong B_p/B_T \cong 0.1$ to the field lines should be equivalent to a poloidally extended rail limiter of height $H' = H + T\theta \approx 5$ cm for Microtor. The approximate poloidal extension of this same limiter when oriented in the vertical direction was $\cong 10$ cm; thus one might expect that the λ in the former case would be larger by $\sim\sqrt{10/5} \sim 1.4$, whereas in fact there appeared to be no significant difference in λ between the two cases. It may be that in this case some other processes are limiting the effective L and masking this difference expected between the two limiter configurations.

4. HEAT DEPOSITION MEASUREMENTS

One expects that the heat flux of $q(W \cdot cm^{-2})$ to an electrically floating surface in contact with the plasma is given by [16]

$$q = \gamma J^+ T_e \qquad (4)$$

where J^+ is the ion saturation current $(A \cdot cm^{-2})$, T_e is the electron temperature (eV) and γ is the heat transmission coefficient. A 1-D sheath potential model (e.g. Ref. [17]) predicts that the sheath drop between the plasma and a floating surface will be $\Delta\phi \cong 3\ kT_e$, so that each ion accelerated through the sheath should deposit $\gtrsim 5\ kT_e$ and each electron which penetrates the barrier should deposit $\gtrsim 2$ kT, implying that $\gamma \sim 8$ for hydrogen. Secondary electron emission at a floating metal surface can reduce $\Delta\phi$ and increase the total heat flux due to electrons such that up to $\gamma \sim 20$ would be expected [18, 19].

Sections 4.1 and 4.2 describe heat deposition measurements in Macrotor and Microtor, respectively, and Sections 4.3 and 4.4 describe some observations of heat deposition asymmetries for Microtor and Macrotor, respectively. These results are discussed in Section 6.3.

4.1. Heat deposition in Microtor

The average heat flux $\bar{q}$ to the tip of the 0.15 cm radius probe was measured (see Section 2) and compared with that expected from the J^+ and T_e values measured using the same tip as a Langmuir probe. Here $\bar{q}$ is defined as the total energy Q deposited onto the tip, integrated over the discharge (see Section 2), divided by the discharge duration ($\cong 20$ ms for Microtor) and the total projected probe area for Microtor ($A \cong 0.3\ cm^2$).

Figure 6 presents the data obtained in this way for a configuration in which the probe is located at the outer equatorial plane, 180° away toroidally from a grounded rail limiter extended toroidally as in Fig.4, case B. The J^+ scrape-off layer thickness is again $\cong 1$ cm in this relatively low-density discharge for which $\bar{n} \cong 5 \times 10^{12}\ cm^{-3}$, and the density near the limiter edge is estimated to be $n \cong 4 \times 10^{11}\ cm^{-3}$. Note that the probe tip was floating for the $\bar{q}$ measurements, but that grounding it did not much affect the results (see r = 7 cm point).

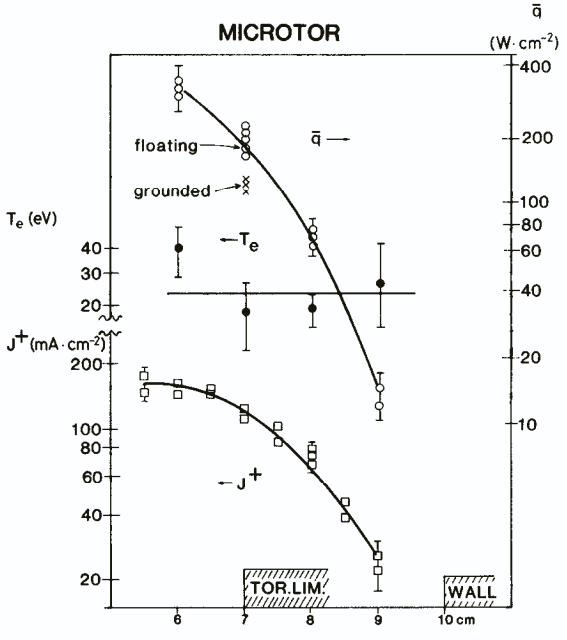

FIG.6. J^+, T_e and $\bar{q}$ measured by a probe 180° toroidally away from a toroidally oriented partial rail limiter (as in Fig.4, case B).

Figure 6 also shows a trend which has been observed before in other tokamaks [14, 20, 21], namely that the J^+ scrape-off thickness λ can be considerably smaller than the electron temperature scrape-off layer thickness λ_T. The reason for this difference is not yet understood; however, since T_e is essentially flat in the scrape-off layer of Microtor, we can, if we like, equate the J^+ scrape-off layer thickness λ with the density scrape-off layer thickness λ_n (through Eq.(1)).

In order to check whether the type of scrape-off results shown in Fig.6 are independent of toroidal angle, another set of measurements of $\bar{q}$, J^+ and T_e was made, using four fixed thermocouple/Langmuir probes mounted on the side of the limiter itself. For these measurements the grounded limiter shown in Fig.4 (case A) was located 1.5 cm inside, past the outer wall, and the probes were facing the electron drift direction. The resulting J^+ profiles again showed $\lambda \cong 1$ cm, while the T_e profiles were essentially flat at $T_e = 30 \pm 10$ eV. The $\bar{q}$ profile showed a pronounced peaking nearest the leading edge of the limiter (i.e. the $\bar{q}$ profile had a scrape-off thickness of $\cong 0.25$ cm), so that in general the results appeared quite similar to those shown in Fig.6.

Since the scrape-off layer thickness for $\bar{q}$ is less than that for J^+, and since T_e does not vary significantly across the scrape-off layer, we conclude that $\bar{\gamma}$ is varying with radius (where the bar refers to the time-average γ). In Fig.7 we plot $\bar{\gamma}$ versus r for the data of Fig.6 and also for the limiter-probe data. For example, the r = 6 cm point in the case of Fig.6 had $\bar{q} = 330$ W·cm^{-2}, $\bar{J}^+ = 0.16$ A·cm^{-2}, and $\bar{T}_e \cong 40$ eV; thus $\bar{\gamma} \cong 50$ with a shot-to-shot variability of $\sim \pm 40\%$. It can be seen that both sets of data result in a calculated $\bar{\gamma}$ which is up to 10 times larger than expected from the sheath model and which apparently falls with radius in the scrape-off layer.

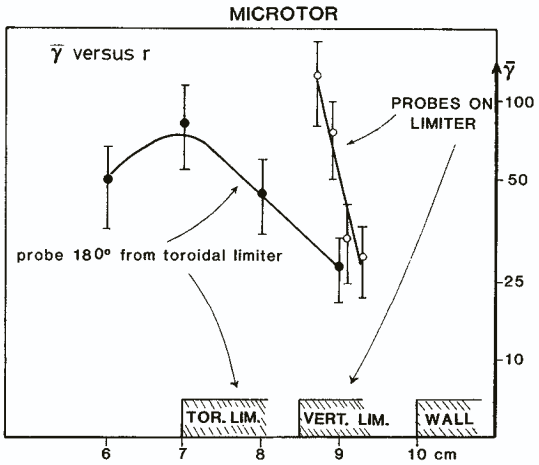

FIG. 7. Calculated heat transmission coefficients $\bar{\gamma}$ versus radius for the data on Microtor. The two cases were run separately with the respective limiter positions indicated on the x-axis.

4.2. Heat deposition in Macrotor

The same movable 0.15 cm radius thermocouple/Langmuir probe was used to measure the heat deposition profile in the limiterless Macrotor as shown in Fig.5. It was again observed that $\bar{q}$ increased more rapidly than did J^+ as the probe was moved toward the centre of the discharge, as was also the case for the Microtor measurements described in the previous section.

An estimate of $\bar{\gamma}$ can be made for the region nearest the centre of the plasma for which $T_e \cong 30$ eV can be inferred from (I, V) traces like those shown in Fig.5(c). At about r = 31 cm (r/a $\cong$ 0.7), we find $\bar{q} \cong 600$ W·cm^{-2} and $J^+ \cong 0.8$ A·cm^{-2} (both evaluated using the total probe area of $\cong 0.5$ cm^2), thus $\bar{\gamma} \cong 25$ for this point. For r > 31 cm, the temperature information is unavailable (because of the very large $\tilde{I}^+/I^+$ in the edge); however, since $\bar{q}$ falls by over a factor of 100 over this profile while J^+ falls by only $\lesssim 3$, it is quite likely that $\bar{\gamma}$ also falls nearer the wall, as was also the case for the limiter scrape-off layers in Microtor (Fig.7).

4.3. Heat deposition asymmetries in Macrotor

There are several possible reasons for the anomalously high $\bar{\gamma} \cong 30$–100 reported in the previous two sections; however, the simplest explanation is that a high-energy runaway or 'epithermal' [16, 22] electron tail with $E \gg kT_e$ was depositing additional energy onto the probes. This is particularly likely for our experiment in which the probes were located at the outer equatorial plane (where runaways are preferably lost) and for which the total heat deposition onto the probes involved only a small fraction ($\sim 10^{-3}$) of the total Ohmic heating power. A special 2 cm × 5 cm electrically grounded double-sided probe was constructed in order to measure separately the heat deposition from the electron 'e' and ion 'i' drift directions (see Fig.8(a)). If high-energy electrons were contributing significantly to $\bar{\gamma}$ then we would expect much larger heat flux from the e direction than from the i direction.

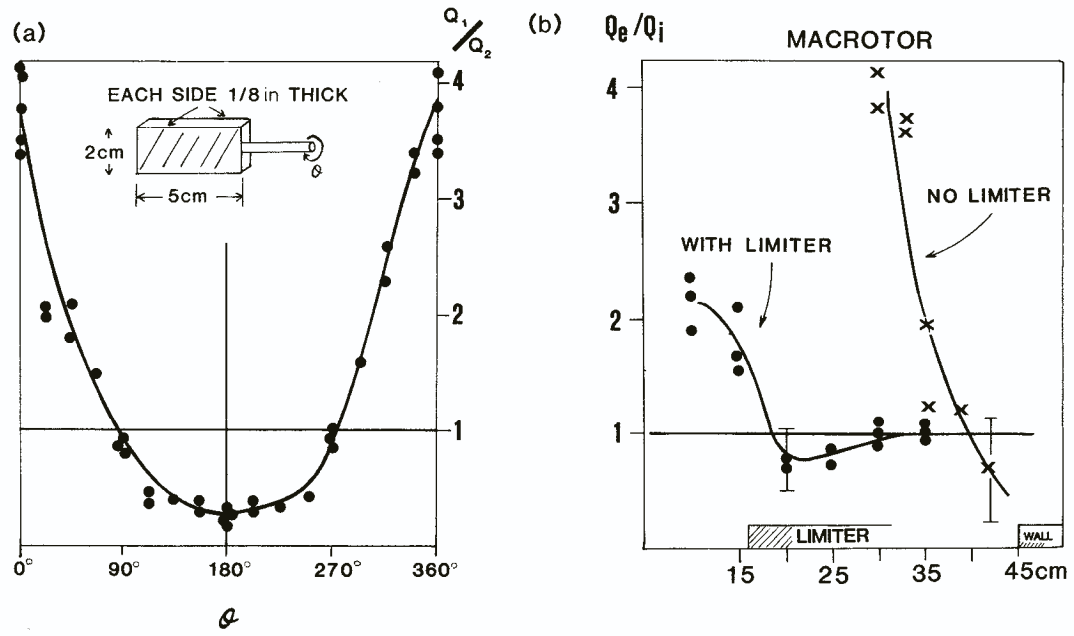

FIG.8. (a) Heat asymmetry ratio Q_1/Q_2 versus angle for the double-sided probe; this shows that probes facing the electron drift side receive about four times more heat than those facing the ion side in Macrotor. (b) Plot of the ratio Q_e/Q_i versus radius with and without a limiter in Macrotor.

Figure 8(a) is a plot of the ratio of the total heat received on one side of the probe, Q_1, to that received on the other side, Q_2, as a function of the probe's angle with respect to the toroidal field. For this run the probe was located at the outer equatorial plane, 15 cm into a limiterless Macrotor discharge, at a point which corresponds to the $r \cong 31$ cm position shown in Fig.5 where the calculated $\bar{\gamma} \cong 25$. For $\theta = 0$, the side facing the electron drift direction (Q_1) receives about four times more heat than does the ion drift side, and as the probe is rotated, the ratio Q_1/Q_2 varies just as would be expected from a directed source of heat flowing from the e direction.

Figure 8(b) is a plot of the radial profiles of Q_e/Q_i as observed with this probe, both with and without a limiter in Macrotor. Without a limiter it is seen that the asymmetry factor falls from $\cong 4$ at $r/a \cong 0.7$ to $\cong 1$ at $r/a = 1$, a result which is reminiscent of the steep decrease in $\bar{q}$ seen by the small probe in the same region of Macrotor (Fig.5). For the case in which a 12 cm high outer limiter was inserted 60° away toroidally from the double-sided probe, the asymmetry factor is seen to drop to ~ 1 as soon as the probe is located more than a few centimeters into the limiter's shadow. This suggests that the asymmetry is caused by a process which has a relatively small scrape-off layer thickness when compared with that of $\lambda \cong 10$ cm for ion flow.

These results seem to be consistent with the idea that a directed high-energy electron population is at least partly responsible for the anomalously high $\bar{\gamma}$. In particular, the scrape-off layer thickness for high-energy runaways to diffuse past the edge of a limiter should be quite small because of their very high parallel velocities (see Eq.(2)) and their high energy (which allows them to cross the sheath potential which repels most of the low-energy electrons).

A test of this possibility was made by attaching to the end of the double-sided probe a grounded stainless steel 'runaway scraper' which extended radially ~0.5 cm past the normal edge of the probe but which was thermally isolated from it. The probe was then inserted up to 15 cm, past the outer limiter, and it was found that in all cases a *symmetrical* heat deposition was then obtained, i.e. $Q_e = Q_i \pm 10\%$. A small localized melting was also observed on the e drift side of the runaway scraper. Thus it seems that for Macrotor the heat asymmetry was due to directed particles which had a scrape-off layer thickness that was very short compared with the ion density scrape-off layer thickness.

4.4. Heat deposition asymmetries in Microtor

The same double-sided heat probe (without the runaway scraper) was used in Microtor to test for e/i asymmetries. A typical value of $Q_e/Q_i \cong 2$ was found when the probe was inserted past the poloidally extended rail limiter (Fig.4, case A). It was also observed that after ≅ 20 Microtor discharges the electron drift side of this probe showed a heavily melted zone within ≅ 2 mm of the edge facing the plasma while the ion drift side was unchanged.

Heat flux asymmetry was also observed using the set of four probes which were fixed into the side of the Microtor limiter (see Section 4.1). When these probes were facing the electron drift direction the heat scrape-off layer thickness was $\lambda_Q \cong 0.2$ cm, while when the limiter was flipped so that the same probes faced the ion drift direction the heat scrape-off thickness was ≅ 0.5 cm. This change in heat deposition occurred without measurable changes in J^+ or T_e between the two sides, again suggesting that at least part of the heat conduction anomaly is due to a small population of directed high-energy electrons.

5. FLUCTUATIONS

Large fluctuations in I^+(and I^- and floating potential ϕ_f) are characteristic of the plasma near the outer equatorial plane of Macrotor [7, 8] and Microtor [9]. The value of $\tilde{I}^+/I^+$ generally increases with r/a and with decreasing density, and is typically $(\tilde{I}^+)_{rms}/I = 0.05$–$0.3$ near the wall and in the scrape-off layer (note that an rms fluctuation level of 0.3–0.4 means a peak fluctuation level of ~ 100% of the mean value).

The spectrum of these I^+ fluctuations is always broadband and usually shows a power law dependence $\tilde{I}^+ \sim f^{-2\pm1}$. The spectral power is mainly below ~ 100 kHz in Macrotor but extends to higher frequencies in Microtor (probably due to the different diamagnetic drift frequencies as for ATC/PLT [23]). There is sometimes a broad peak in the spectrum at f ~ 20–40 kHz in Macrotor and at f ~ 100–300 kHz in Microtor.

The autocorrelation time for I^+ is always small (~ 1–10 μs), indicating a 'turbulent' character. The radial correlation length L_r of I^+ in Macrotor is $\lesssim 1$ cm. Ion saturation current signals from the four probes on the side of the vertical limiter in Microtor also indicate that L_r is $\lesssim 1$ cm in the scrape-off layer of this machine.

It is a striking fact that the I^+ fluctuations observed in the limiter scrape-off layer are quite similar to those observed in the edge of a limiterless discharge (compare Figs 2 and 5). The most important variable for determining the relative fluctuation level seems to be the local density, i.e. roughly $\tilde{I}^+/I^+ \propto n^{-0.5}$.

6. DISCUSSION

Section 6.1 reviews the relationships between these results and some previous experiments on tokamak edge properties; in Section 6.2 we discuss possible causes for the particle scrape-off layer behaviour described in Section 3; in Section 6.3 we discuss possible causes for the heat-flux behaviour described in Section 4; and our conclusions are outlined in Section 7.

6.1. Relationships to previous experiments

A summary of some of the previous measurements of edge-plasma properties is given in Table I (see references listed there). It can be seen that the values of T_e and n_e obtained for Macrotor and Microtor are within the range of values obtained in other machines; however, there is quite a large variability so that a simple, precise generalization of these results is not possible at this stage. Some of this variability is naturally due to the differing configurations and bulk plasma conditions; for example, the highest edge density is observed for the machine with the highest average density (Alcator). A thorough interpretative review of probe measurements in the tokamak boundary layer has recently been given by Staib [14].

Of particular interest for a comparison between different experiments are the values derived for the particle cross-field diffusion coefficient $D_\perp$ and for the heat transmission coefficient γ. Generally, $D_\perp$ as evaluated in the scrape-off layer using Eq.(2) is approximately given by

$$D_\perp \sim D_{Bohm} \cong 6.25 \times 10^6 T(eV)/B(G)\ cm^2 \cdot s^{-1}$$

This formula seems to hold for high-field (e.g. Alcator [24]), medium-field (e.g. JFT-II [20]) and low-field (e.g. Macrotor) machines. There is also some indication of a Bohm-type temperature scaling [14].

Information about the scrape-off thickness is also directly useful for the design of limiters in present-day tokamaks [11, 12, 14]. On PLT it was deduced from the limiter damage pattern that λ for runaways was

TABLE I. REPRESENTATIVE VALUES FOR EDGE-PLASMA PROPERTIES OF SOME TOKAMAKS

Device [Ref.]	Boundary	B_T(T)	R(cm)	a(cm)	T_e(eV)	n_e(cm^{-3})	λ_n(cm)	λ_T(cm)	λ_Q(cm)	$D_\perp/D_{Bohm}$	$\tilde{n}/n$	γ
Alcator [24, 32]	poloidal limiter	6.0	60	10	10–12	7×10^{13}	~1			$\gtrsim 1$	$\lesssim 0.5$	
ASDEX [14]	poloidal divertor	2.0	165	40	30	$<3\times10^{11}$	2.5	$\gg 2.5$				
Caltech [33, 42]	outer limiter	0.36	45	16	10–25	$10^{11}-10^{12}$	1.5	1.5		~1	~0.2	
DITE [28, 41, 43]	bundle divertor	0.9–2.7	117	19–26	~25	$\sim10^{12}$	~5				0.08–1.0	6–200
DITE [34, 35, 40]	poloidal limiters	1.4–2.7	117	26	5–15	$<2.5\times10^{12}$	~1–3	2–8				
DIVA [16, 22, 26]	poloidal divertor	0.8–2.0	60	10	15–80	$1-5\times10^{12}$				~0.1		15–20
JFT-II [20, 27, 36]	rail limiters	1.7	90	25	30–50	$2-5\times10^{12}$	1.5–4.5	$\gg 4$	1.5–4.5	~1	$\gtrsim 0.1$	3–20
Macrotor [this paper]	rail limiter	0.3	90	45	20–40	$\sim10^{11}-10^{12}$	~7–10			~2	0.05–0.3	~25
Microtor [this paper]	rail limiter	2.0	30	10	20–40	$\sim10^{11}-10^{12}$	~1	$\gg 1$	0.2–0.5	~0.5	0.05–0.3	30–120
PDX [21, 29]	limiter or divertor	1.9	145	39	7–15	3×10^{10}–3×10^{12}	2–4	15	0.5–2.5			
PLT [21, 25, 29, 37]	mushroom limiters	1.7–1.9	130	40	5–40	$<6\times10^{11}$	~4	~15	~0.1–0.2			
T-12 [38]	poloidal divertor	0.8	36	8	20–60	$<10^{12}$	<1	$\gg 1$		$\gtrsim 0.1$		40–100
TFR 600 [12, 37, 39]	limiters	4.0	98	19	~10	$\sim7\times10^{12}$	~1.8	$\gg 2$		$\gtrsim 1$		~15

smaller than λ for the thermal plasma (which in turn was smaller than λ for the fast ions from neutral beam injection) [25], a behaviour which appears to be similar to that described for Macrotor and Microtor in Sections 4.3 and 4.4.

Studies of the heat transmission coefficient γ are fewer than those of λ, the most detailed having been done on DIVA [16, 26], JFT-II [27] and DITE [28]. In all of these cases an anomalously high γ has been reported for at least some discharge types, particularly for low-density discharges which had an epithermal or runaway electron tail [16, 28] and associated heat-flux asymmetry. On PLT, however, it was observed that more heat was arriving onto a calorimeter probe from the ion side than from the electron side [29], a result which is not yet understood.

Strong broadband fluctuations in I^+ and ϕ_f have also been observed in several tokamaks besides Macrotor and Microtor (see Table I). Striking evidence for such fluctuations has recently come from high-speed movies of the visible light emission in ASDEX [30–31] and Dite [30], which show strong small-scale 'filamentation' occurring in the edge plasma throughout the discharge. Strong $\tilde{n}/n \cong 1$ edge fluctuations have also been observed in Alcator using CO_2 laser scattering [32].

Several other experimental results are referred to in Table I (Refs [33–43]). These generally reproduce the previously cited results on edge-plasma parameters, diffusion, heat transmission and fluctuations.

6.2. Particle transport models

The radial particle diffusion coefficients $D_\perp \cong D_{Bohm}$ estimated for the limiter shadow regions of Macrotor and Microtor (Section 3) appear to be highly 'anomalous' when compared with the collisional cross-field diffusion coefficient $D_\perp \cong q^2 \nu_{ei} \rho_e^2$. There are at least two possible mechanisms which might result in such a large radial particle transport, namely radial $\tilde{E}_p \times B_T$ drifts driven by electrostatic fluctuations or radial $\tilde{B}_r$ perturbations along which particles can freely flow across the toroidal field.

Radial magnetic field fluctuations would need to be extremely large in order to move an ion across the field by a distance λ during a time $\tau_\parallel$ set by the ion residence time in the limiter shadow. An average radial velocity $\bar{v}_r \cong \lambda/\tau_\parallel$ would be required, which, if produced by ion motion at an angle B_r/B_T to the toroidal field, would require

$$B_r/B_T \cong \frac{\lambda}{L} \qquad (5)$$

where L is the average distance which a (collisionless) ion travels along the field in the scrape-off layer (see Eq.(2)). Thus for $\lambda \cong 10$ cm and $L \cong q\pi R$ (for a rail limiter) an average $B_r/B_T \cong 0.10/12 \cong 10^{-3}$ would be required, which is considerably larger than the observed $\tilde{B}_r/B_T \cong 10^{-5}$ for broadband fluctuations in the edge region of Macrotor [8].

Radial particle transport due to electrostatic fluctuations depends on the net $\langle \tilde{n} \cdot \tilde{v}_r \rangle$ flux, where $\tilde{v}_r$ comes from the $\tilde{E}_p \times B$ drift; thus a measurement of $\tilde{n}$ alone is not sufficient to estimate the magnitude of the cross-field transport. However, it is well known that a large turbulent level of $\tilde{n}/n \gtrsim 1$ such as observed in these experiments can readily cause Bohm-type diffusion [11, 14]. The stability properties of the edge plasma are currently under investigation in order to try to calculate edge-plasma diffusion coefficients; in particular, two of the most highly developed theoretical treatments are those involving the rippling mode [44–46] or the collisional drift wave [46, 47], both modes having been shown to be unstable for typical tokamak edge parameters. A thermal instability which involves current filamentation [48], and the possible instability due to supersonic flow [49], or contact with the wall or limiter [14] are other candidates for explaining edge-plasma instability and diffusion.

Overall, it seems quite likely that the particle scrape-off layer properties of tokamak edges are caused by some sort of electrostatic turbulence. Although a recent measurement of $\tilde{n}$ and $\tilde{E}_p$ and the associated $\langle n \cdot v_r \rangle$ flux in the edge plasma has indicated that this turbulence-induced flux can indeed be very large [33], a conclusive connection between turbulence and edge transport has not yet been made.

6.3. Heat flux models

The measurements described in Section 4 have indicated the presence of an anomalously large heat transmission to small probes near the outside edge of the plasma, i.e. $\gamma \sim 30–100$ instead of the simple sheath model prediction of $\gamma \cong 8$ [17, 50]. This is most clearly seen in the Microtor results of Fig.7.

At least part of this anomaly is evidently associated with asymmetrically deposited fast electrons which are not accounted for in the simple sheath model. The measured e/i side asymmetry ratio of 2–4 (Section 4.3) would at first seem too small to explain the overall γ anomaly. However, the asymmetry ratio was measured with a relatively large probe (2 cm × 5 cm), so that if the fast electrons had a very small scrape-off thickness (as was indicated in Sections 4.3 and 4.4)

the asymmetry ratio for the small probe could have been high enough (i.e. 60–200) to explain the whole γ anomaly. Unfortunately, the asymmetry ratio and γ were not measured with the same probe, so that the extent of a possible symmetrical component to the γ anomaly remains unresolved.

There are some other possible modifications to the simple sheath model which could help explain that part of the γ anomaly which may not be associated with fast electrons: (1) secondary electron emission; (2) fluctuation effects; (3) arcing; and (4) non-ambipolar effects.

Secondary electron production at the probe may reduce the floating potential and so increase the heat transmission coefficient up to $\gamma \sim 20$ [16, 18, 19]. However, this large effect only occurs when the ratio of secondary electron current to incident ion current is $\lesssim 3$, which is unlikely to occur at $T_e \lesssim 50$ eV in these experiments. The apparent insensitivity of $\bar{q}$ to the switch from a floating probe to a grounded one (Fig.6) indirectly suggests that ϕ_f is not a sensitive variable in determining $\bar{q}$. A direct measurement of secondary electron emission or of $\bar{q}(\phi)$ has not been made here.

The second feature which is not accounted for in the sheath model is the fact that $e\tilde{\phi}/kT_e \lesssim 1$ at the edge, thus an average $\bar{q} = \int \bar{q}(\phi)\, P(\phi)\, d\phi$ is appropriate (where $P(\phi)$ is the probability distribution of ϕ). Since the heat flux $q(\phi)$ is a minimum at $\phi \cong \phi_f$, it seems likely that fluctuations in ϕ will tend to increase γ.

If the local potential becomes too high, arcing to the probe can occur [51, 52]. Fern-type arcs are commonly observed on the grounded probe shafts, but these are most likely associated with disruptive instabilities. Microscopic arcs remain a possible source of enhanced heat deposition; however, their existence is not visible on the Langmuir probe characteristic at least at $f < 100$ kHz.

Non-ambipolar flow to the limiter has been shown [53] to allow increased electron heat flow to the leading edge of a limiter, similarly to that described in Fig.7. Some evidence for non-ambipolar flow to a tokamak limiter has recently been reported [54].

Overall, it seems most likely that the anomalously high heat transmission coefficients observed in these experiments are due to a relatively small population of asymmetrically deposited fast electrons, although the influence of other effects cannot as yet be ruled out. It should be noted that the effect of fast electrons on the γ anomaly may be specific to small probes near the outside major radius side of the chamber where the relatively small fast electron population would be preferably lost [55].

7. CONCLUSIONS

(a) Plasma scrape-off layer thicknesses in the limiter shadow were $\lesssim 10$ cm in Macrotor at 0.3 T and ~ 1 cm in Microtor at 2 T, both at $n \sim 10^{11} - 10^{12}$ cm^{-3} and $T_e \sim 20 - 40$ eV. These results correspond to a particle diffusion coefficient on the order of $0.5 - 2\, D_{Bohm}$.

(b) Broadband turbulent fluctuations are present in the edge region, both in front of and in the shadow of the limiter. Typically, $(\tilde{I}^+)_{rms}/I^+ \sim 0.05 - 0.3$ for the edge regions of both machines.

(c) Small Langmuir/thermocouple probes located near the outside equatorial plane showed an anomalously large heat transmission coefficient, $\gamma \sim 30 - 100$, instead of the $\gamma \cong 8$ expected from the simple sheath model.

(d) Asymmetrical heat deposition was observed, with $\sim 2 - 4$ times more heat deposited on the electron drift side than on the ion drift side. This asymmetry can be removed by attachment of a small runaway electron dump on the heat probe.

(e) The anomaly in γ and the asymmetry in heat deposition are largest at points nearest the limiter edge, indicating that these anomalies are at least in part associated with a species with an unusually small scrape-off layer, e.g. runaway electrons.

(f) The anomalous particle diffusion in the edge region is most likely caused by the large level of electrostatic turbulence observed there.

(g) The anomalous heat deposition in these experiments is most likely caused by fast electrons, although perhaps not all of the γ anomaly is associated with such an asymmetrical heat flux.

There are many refinements of experimental technique and theoretical modelling which will be necessary to better understand the edge plasma; for example, time-resolved heat flux measurements [29, 34], multiple-probe edge profile measurements [35], improved modelling of the probe heat transmission coefficient [56], inclusion of atomic physics processes [57], and better understanding of the physical processes occurring in the scrape-off layer [58] and sheath [59]. Perhaps most significant to future tokamak operation will be the task of accounting for all the heat and particle flows to the various parts of the chamber wall or divertor, and then learning how to actively control these flows to achieve optimum performance.

ACKNOWLEDGEMENT

The authors wish to thank Prof. R.W. Conn and his group for helpful discussions about tokamak edge problems.

REFERENCES

[1] KEILHACKER, M., DAYBELGE, U., Nucl. Fusion **21** (1981) 1497.
[2] CONN, R.W., SVIATOSLAVSKY, I.N., SZE, D.K., in Engineering Problems of Fusion Research (Proc. 8th IEEE Symp. San Francisco, 1979) Vol.1 (1979) 568.
[3] CHEN, F.F., in Plasma Diagnostic Techniques (HUDDLESTONE, R.H., LEONARD, S.K., Eds), Academic Press, New York (1975) 113.
[4] MOTLEY, R.W., Q-Machines, Academic Press, New York (1975) 29.
[5] LAFRAMBOISE, J.F., RUBINSTEIN, J., Phys. Fluids **19** (1976) 1900.
[6] BROWN, I.G., COMPHER, A.B., KUNKEL, W.B., Phys. Fluids **14** (1971) 1377.
[7] ZWEBEN, S.J., MENYUK, C.R., TAYLOR, R.J., Phys. Rev. Lett. **42** (1979) 1270.
[8] ZWEBEN, S.J., TAYLOR, R.J., Nucl. Fusion **21** (1981) 193.
[9] SEMET, A., MASE, A., PEEBLES, W.A., LUHMANN, N.C., ZWEBEN, S.J., Phys. Rev. Lett. **45** (1980) 445.
[10] ZWEBEN, S.J., MENYUK, C.R., TAYLOR, R.J., Rev. Sci. Instrum. (1979) 972.
[11] McCRACKEN, G., STOTT, P.E., Nucl. Fusion **19** (1979) 887.
[12] TFR Group, Association Euratom-CEA, Centre d'études nucléaires de Fontenay-aux-Roses, Rep. EUR-CEA-FC-1114 (1981).
[13] OGDEN, J.M., SINGER, C.E., POST, D.E., JENSEN, R.V., SEIDL, F.G.P., IEEE Trans. Plasma Sci. **PS-9** 4 (1981) 274.
[14] STAIB, P., J. Nucl. Mater. **111** and **112** (1982) 109.
[15] COHEN, S.A., J. Nucl. Mater. **77** and **78** (1978) 68.
[16] KIMURA, H., MAEDA, H., UEDA, N., SEKI, M., KAWAMURA, H., YAMAMOTO, S., NAGAMI, M., ODAJIMA, K., SENGOKU, S., SHIMOMURA, Y., Nucl. Fusion **18** (1978) 1195.
[17] EMMERT, G.A., WIELAND, R.M., MENSE, A.T., DAVIDSON, J.N., Phys. Fluids **23** (1980) 803.
[18] HARBOUR, P.J., HARRISON, M.F.A., Nucl. Fusion **19** (1979) 695.
[19] FUCHS, G., NICOLAI, A., Nucl. Fusion **20** (1980) 1247.
[20] UEHARA, K., GOMAY, Y., YAMAMOTO, T., SUZUKI, N., MAENO, M., HIRAYAMA, T., SHIMADA, M., KONOSHIMA, S., FUJISAWA, N., Plasma Phys. **21** (1979) 89.
[21] BUDNY, R., J. Vac. Sci. Technol. **20** 4 (1982) 1238.
[22] YAMAMOTO, S., SENGOKU, S., KIMURA, H., SHIMOMURA, Y., MAEDA, H., OHTSUKA, K., ODAJIMA, M., NAGAMI, M., UEDA, N., Nucl. Fusion **18** (1978) 205.
[23] MAZZUCATO, E., Phys. Fluids **21** (1978) 1063.
[24] SCATURRO, L., KUSSE, B., Nucl. Fusion **18** (1978) 1717.
[25] COHEN, S.A., BUDNY, R., McCRACKEN, G.M., ULRICKSON, M., Nucl. Fusion **21** (1981) 233.
[26] DIVA GROUP, Nucl. Fusion **18** (1978) 1619.
[27] GOMAY, Y., FUJISAWA, N., MAENO, M., SUZUKI, N., UEHARA, K., YAMAMOTO, T., KONOSHIMA, S., Nucl. Fusion **18** (1978) 849.
[28] ERENTS, S.K., FIELDING, S.J., GILL, R.D., GOODALL, D.H.J., HARBOUR, P.J., et al., in Plasma Physics and Controlled Nuclear Fusion Research 1980 (Proc. 8th Int. Conf. Brussels, 1980) Vol.1, IAEA, Vienna (1981) 697.
[29] MANOS, D.M., BUDNY, R., SATAKE, T., COHEN, S.A., J. Nucl. Mater. **111** and **112** (1982) 130.
[30] GOODALL, D.H.J., J. Nucl. Mater. **111** and **112** (1982) 11.
[31] NIEDERMEYER, H. (Asdex), private communication, 1982.
[32] SLUSHER, R.E., SURKO, C.M., Phys. Rev. Lett. **23** (1980) 472.
[33] ZWEBEN, S.J., LIEWER, P.C., GOULD, R.W., J. Nucl. Mater. **111** and **112** (1982) 39.
[34] STANGEBY, P.C., McCRACKEN, G.M., VINCE, J.E., J. Nucl. Mater. **111** and **112** (1982) 81.
[35] PROUDFOOT, G., HARBOUR, P.J., J. Nucl. Mater. **111** and **112** (1982) 87.
[36] OHTSUKA, H., KIMURA, H., SHIMOMURA, S., MAEDA, H., YAMAMOTO, S., NAGAMI, M., UEDA, N., KITSUNEZAKI, A., NAGASHIMA, T., Plasma Phys. **20** (1978) 749.
[37] STAUDENMEYER, G., STAIB, P., BEHRISCH, R., Nucl. Fusion **20** (1980) 96.
[38] BORTNIKOV, A.V., BREVNOV, N.N., GERASIMOV, S.N., ZHUKOVSKIJ, V.G., KUZNETSOV, N.V., NAFTULIN, S.M., PERGAMENT, V.I., KHIMCHENKO, L.N., in Plasma Physics and Controlled Nuclear Fusion Research 1980 (Proc. 8th Int. Conf. Brussels, 1980) Vol.1, IAEA, Vienna (1981) 687.
[39] TFR GROUP, J. Nucl. Mater. **93** and **94** (1980) 272.
[40] PROUDFOOT, G., HARBOUR, P.J., J. Nucl. Mater. **93** and **94** (1980) 413.
[41] PAUL, J.W.M., in Controlled Fusion and Plasma Physics (Proc. 9th Europ. Conf. Oxford, 1979) Vol.2, UKAEA, Culham Lab., Abingdon (1979) 371.
[42] ZWEBEN, S.J., LIEWER, R.W., GOULD, R.W., Local magnetic divertor for control of the plasma-limiter interaction in a tokamak, submitted to Phys. Fluids.
[43] STOTT, P.E., WILSON, C.M., GIBSON, A., Nucl. Fusion **18** (1978) 475.
[44] CALLEN, J.D., EMMERT, G.A., BAILEY, A.M., BENCHIKH-LEHOCINE, M.E., DAVIDSON, J.N., et al., in Plasma Physics and Controlled Nuclear Fusion Research 1980 (Proc. 8th Int. Conf. Brussels, 1980) Vol.1, IAEA, Vienna (1981) 775.
[45] CALLEN, J.D., CARRERAS, B.A., DIAMOND, P.H., BENCHIKH-LEHOCINE, M.E., GARCIA, L., HICKS, H.R., in Plasma Physics and Controlled Nuclear Fusion Research 1982 (Proc. 9th Int. Conf. Baltimore, 1982) Vol.1, IAEA, Vienna (1983) 297.
[46] HASSAM, A.B., DRAKE, J.F., Phys. Fluids **26** (1983) 113.
[47] HASEGAWA, A., WAKATANI, M., Plasma Edge Turbulence (submitted for publication).

[48] TOMIMURA, A., HAINES, M.G., J. Plasma Phys. 23 (1980) 1.
[49] STANGEBY, P.C., Nucl. Fusion 22 (1982) 1383.
[50] HOBBS, G.D., WESSON, J.A., Plasma Phys. 9 (1967) 85.
[51] GOODALL, D.H.G., McCRACKEN, G.M., Nucl. Fusion 19 (1979) 1396.
[52] MAENO, H., OHTSUKA, H., YAMAMOTO, S., YAMAMOTO, T., SUZUKI, N., FUJISAWA, N., OGIWARA, N., Nucl. Fusion 20 (1980) 1415.
[53] STRAWICH, C.M., EMMERT, G.A., Nucl. Fusion 21 (1981) 1291.
[54] IVANOV, R.S., NEDOSPASOV, A.V., FIDELIMAN, G.N., in Controlled Fusion and Plasma Physics (Proc. 10th Europ. Conf. Moscow, 1981) (1981) paper J-3.
[55] KNOEPFEL, H., ZWEBEN, S., Phys. Rev. Lett. 35 (1975) 1340.
[56] STANGEBY, P.C., J. Phys., D. (London). Appl. Phys. 5 (1982) 1007.
[57] PETRAVIC, M., HEIFETZ, D., POST, D., LANGER, W., SINGER, C., in Plasma Physics and Controlled Nuclear Fusion Research 1982 (Proc. 9th Int. Conf. Baltimore, 1982) Vol.1, IAEA, Vienna (1983) 323.
[58] SINGER, C.E., LANGER, W.D., Axisymmetric Tokamak Scrape-off Transport, Princeton Plasma Physics Lab. Rep. PPPL-1920 (Aug.1982).
[59] DAYBELGE, U., BEIN, B., Phys. Fluids 24 (1981) 1190.

(Manuscript received 16 July 1982
Final manuscript received 20 January 1983)